Measurements of differential scattering cross section using a ring transducer

Tomas T. Jansson[a)]
Department of Electrical Measurements, Lund University, P.O. Box 118, 221 00 Lund, Sweden

T. Douglas Mast[a)]
Applied Research Laboratory, The Pennsylvania State University, University Park, Pennsylvania 16802

Robert C. Waag
Departments of Electrical Engineering and Radiology, University of Rochester, Rochester, New York 14627

(Received 20 June 1997; accepted for publication 10 February 1998)

A procedure for the measurement of intrinsic scattering object properties is presented and used to obtain illustrative results. The procedure is based on the measurement of the scattered acoustic field as a function of scattering angle and frequency. Measurements are normalized using analytically determined expressions for emitter and detector beams resulting from a combination of unfocused linear elements arranged in a circular configuration. The spatial effects of finite emitter pulse length and detector gate length are represented by a convolution formula valid for narrow-band transmitted signals and long receiver gates. The normalization includes correction for target absorption as well as measurement of the directly transmitted acoustic power in the free field and yields the average differential scattering cross section per unit volume. Under the Born approximation, this quantity is directly proportional to the spatial-frequency spectrum of the scattering medium inhomogeneities. Measured results are reported for two phantoms consisting of glass microspheres embedded in a weakly absorbing agar background medium. For the phantoms employed, scattering effects, rather than increased absorption, are shown to account for most of the difference in transmission loss between pure agar and agar with glass spheres. The measured differential scattering cross sections are compared with theoretical cross sections for distributions of glass spheres measured experimentally. The measured values show good relative agreement with theory for varying angle, frequency, and phantom properties. The results are interpreted in terms of wave space resolution and the potential for tissue characterization using similar fixed transducer configurations. [S0001-4966(98)00306-3]

PACS numbers: 43.20.Fn, 43.20.Ye, 43.80.Ev [JEG]

INTRODUCTION

Normal and diseased tissues have been shown to have different ultrasonic scattering properties under some circumstances.[1–5] These differences arise because varying tissue morphology results in different spatial-frequency spectra, which in turn, can be directly correlated to the average differential scattering cross section per unit volume, i.e., the average power scattered from a unit volume of tissue into some angle relative to the incident beam direction, per unit incident intensity and unit solid angle. The apparent relationship between tissue morphology and ultrasonic scattering properties has led many investigators to measure ultrasonic scattering properties of different tissue types.

Studies concerned with measurements of scattering cross section have mainly been concentrated on the backscatter case[6–19] since this is the most commonly used configuration in clinical practice. However, backscatter measurements are inherently limited in the range of spatial frequencies that can be investigated, since the only parameter that can be varied is the temporal frequency. To increase the range of possible spatial frequencies examined, the angle between emitter and detector can also be varied.[20–25] Such measurements have previously been undertaken using time-consuming physical translation of single-element transducers and have also been limited by the beam patterns produced by the transducers that were utilized.

In our experiments, a transducer array with narrow elements arranged in a circle has been used to overcome these limitations for *in vitro* measurements of scattering cross section. The ring array conveniently allows scanning at arbitrary angles between emitter and detector as well as beamforming using multi-element apertures. The fixed nature of this array allows scattering cross sections to be measured through ensemble averaging of many medium realizations, resulting in measurements with low bias and variance.

A commonly used identity in measurements and analysis of weak scattering is that the spatial-frequency spectrum of the medium variations is proportional to the average differential scattering cross section; that is, that

$$\bar{\sigma}_d(\mathbf{K}) = \frac{k_0^4}{2\pi} S_\gamma(\mathbf{K}), \tag{1}$$

where $\bar{\sigma}_d(\mathbf{K})$ is the differential scattering cross section per unit volume for the scattering vector $\mathbf{K}$, k_0 is the wave number, and $S_\gamma(\mathbf{K})$ is a spatial-frequency spectrum of the me-

[a)]Work performed while at the Ultrasound Research Laboratory, University of Rochester, Rochester, NY.

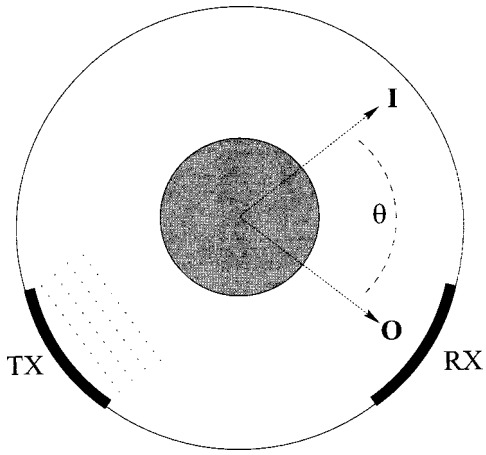

FIG. 1. Scattering configuration. A transmitting aperture (TX) emits a pulse. The scattered wave is then received by a receive aperture (RX). The scattering angle θ is defined as the angle between the corresponding vectors **I** and **O**.

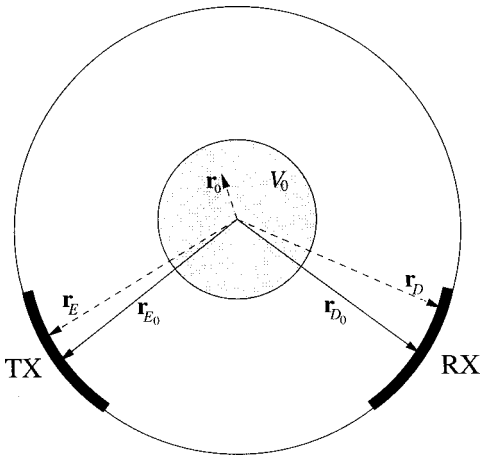

FIG. 2. Geometry for evaluation of scattering integrals. The fixed vectors $\mathbf{r}_{E_0}$ and $\mathbf{r}_{D_0}$, which are directed from the origin to the centers of the emitter and detector, respectively, are indicated by solid lines. The vector $\mathbf{r}_0$, indicated by a dashed line, corresponds to an arbitrary point within the scattering volume V_0, indicated by shading. The vectors $\mathbf{r}_E$ and $\mathbf{r}_D$, indicated by dashed lines, are directed from the origin to arbitrary points on the emitter surface and the detector surface, respectively.

dium variations.[26] However, the differential scattering cross section can only be determined approximately in a practical measurement situation employing finite apertures and time gates. Earlier work has shown that these effects can be removed by normalization of the measured data,[20–23] although the accuracy of the normalization is fundamentally limited by blurring effects associated with the finite measurement system.[25]

In the present study, a normalization procedure applicable to unfocused linear arrays and phased arrays is developed. The procedure analytically incorporates beam patterns of apertures composed of multiple line sources, spatial effects of the emitter pulse and detector gate lengths, and compensation for absorption in the scattering medium. This procedure is specifically applied to the ring transducer system used in our experiments.

In Sec. I, an overview of the normalization theory is given. To verify the validity of the method, measurements were performed on two glass sphere-agar phantoms. The production of these and the method for data collection is presented in Sec. II. Experimental results are presented and compared with theory in Sec. III, and a discussion of the applicability of the present methods to practical tissue characterization is presented in Sec. IV.

I. THEORY

The scattering configuration of our ring transducer system is sketched in Fig. 1. A transmitting aperture emits a wave that propagates in the direction corresponding to the vector **I**, and a receiving aperture records the scattered wave that propagates in the direction corresponding to the vector **O**. Both the vectors **I** and **O** have magnitudes equal to the wave number k_0. The vector $\mathbf{K}=\mathbf{I}-\mathbf{O}$ describes the spatial-frequency content of the scattered wave at the scattering angle θ, which is equal to the angle between **I** and **O**.

The inhomogeneous scattering medium is represented below as a continuous fluid with compressibility and density variations γ_κ and γ_ρ as defined in Ref. 26. For such a fluid, when the scattered amplitude is sufficiently small that the Born approximation is applicable, the scattered acoustic pressure is given by the integral equation[27]

$$p_s(\mathbf{r},t)=-\frac{1}{4\pi}\int\int\int_{V_0}\frac{1}{R}\left\{\frac{\gamma_\kappa(\mathbf{r_0})}{c^2}\frac{\partial^2 p_i(\mathbf{r}_0,t-R/c)}{\partial t^2}+\boldsymbol{\nabla}_0[\gamma_\rho(\mathbf{r}_0)\boldsymbol{\nabla}_0 p_i(\mathbf{r}_0,t-R/c)]\right\}d^3r_0, \tag{2}$$

where c is the background speed of sound, $R=|\mathbf{r}-\mathbf{r}_0|$, and p_s is the scattered pressure observed at a position $\mathbf{r}$. The integration volume V_0 includes the entire support of γ_κ and γ_ρ.

The incident pressure p_i associated with a portion of an ultrasonic array can be approximated as the radiated pressure associated with a vibrating surface in a rigid baffle.[28] For a surface A_E with a normal velocity component having spatial dependence a_E and temporal dependence W_E, such that $\dot{v}(\mathbf{r},t)=a_E(\mathbf{r})W_E(t)e^{-i\omega_0 t}$, where the envelope W_E is slowly varying, the incident pressure is given by

$$p_i(\mathbf{r}_0,t)=\frac{\rho e^{-i\omega_0 t}}{2\pi}W_E(t-|\mathbf{r}_0-\mathbf{r}_{E_0}|/c)\times\left[\int\int_{A_E}\frac{a_E(\mathbf{r}_E)e^{ik_0|\mathbf{r}_0-\mathbf{r}_E|}}{|\mathbf{r}_0-\mathbf{r}_E|}d^2r_E\right], \tag{3}$$

where $\mathbf{r_E}$ is a vector from the origin to an arbitrary point on the emitter surface, and k_0 is the wave number ω_0/c. Expression of the emitter time gate effect is simplified in Eq. (3) by the approximation $|\mathbf{r}_0-\mathbf{r}_E|\approx|\mathbf{r}_0-\mathbf{r}_{E_0}|$, where $\mathbf{r}_{E_0}$ is the vector from the origin to the center of the transducer surface. The integral term in Eq. (3) (i.e., the spatial dependence of the incident pressure) will be denoted $I_E(\mathbf{r}_0)$. The vectors employed in Eq. (3), as well as corresponding vectors defined for the detector, are sketched in Fig. 2.

Substituting Eq. (3) into Eq. (2), integrating by parts, and making use of Green's theorem yields an expression for the scattered pressure valid for slowly varying W_E:

$$p_s(\mathbf{r},t)=\frac{\rho k_0^2 e^{-i\omega_0 t}}{8\pi^2}\int\int\int_{V_0}\frac{e^{ik_0R}}{R}\times W_E(t-R/c-|\mathbf{r}_0-\mathbf{r}_{E_0}|/c)\times(\gamma_\kappa+\mathbf{i}\cdot\mathbf{o}\,\gamma_\rho)I_E(\mathbf{r}_0)d^3r_0. \quad (4)$$

This expression has employed the approximations $|\mathbf{r}_0-\mathbf{r}_E|\approx|\mathbf{r}_E|-\mathbf{i}\cdot\mathbf{r}_0$ for $|\mathbf{r}_E|\gg|\mathbf{r}_0|$ and $|\mathbf{r}-\mathbf{r}_0|\approx|\mathbf{r}|-\mathbf{o}\cdot\mathbf{r}_0$ for $|\mathbf{r}|\gg|\mathbf{r}_0|$, where $\mathbf{i}$ is a unit vector in the propagation direction of the incident wave and $\mathbf{o}$ is a unit vector in the direction of the field point $\mathbf{r}$. The length R is equal to $|\mathbf{r}-\mathbf{r}_0|$.

The received signal is now defined as the Fourier transform of the time dependent scattered wave integrated over the surface A_D of a pressure-sensitive detector with a gate function $W_D(t)$ and a sensitivity function $a_D(\mathbf{r})$. This integration can be written:

$$N(\omega)=\int_{-\infty}^{\infty}e^{i\omega t}\,W_D(t)\times\left[\int\int_{A_D}p_s(\mathbf{r}_D,t)a_D(\mathbf{r}_D)\,d^2r_D\right]dt, \quad (5)$$

where $p_s(\mathbf{r}_E)$ is given by Eq. (4).

Evaluation of Eq. (5) at the frequency $\omega=\omega_0$ yields the result

$$N(\omega_0)=\frac{\rho k_0^2}{8\pi^2}\int\int\int_{V_0}I_D(\mathbf{r}_0)\tau(\mathbf{r_0})\gamma(\mathbf{r}_0)I_E(\mathbf{r}_0)d^3r_0. \quad (6)$$

Here, the function τ represents the spatial effect of emitter and detector time gates defined by the windows W_E and W_D, each of which is nominally centered at $t=0$. This function, which expresses a spatially dependent weighting of effective scattering sources caused by the combination of emitter and detector gates, is given by the convolution integral

$$\tau(\mathbf{r_0})=\int_{-\infty}^{\infty}W_E(t)W_D(t+|\mathbf{r}_{D_0}-\mathbf{r}_0|/c+|\mathbf{r}_0-\mathbf{r}_{E_0}|/c-|\mathbf{r}_{D_0}|/c-|\mathbf{r}_{E_0}|/c)\,dt. \quad (7)$$

In Eq. (7), the delay $|\mathbf{r}_{D_0}|/c+|\mathbf{r}_{E_0}|/c$ in the argument of the detector gate accounts for the two-way propagation time of a wave traveling from the emitter center to the origin and back to the detector center.

In Eqs. (6) and (7), the scattered pressure from Eq. (4) has been used. The inhomogeneity of the medium is represented by $\gamma=\gamma_\kappa+\mathbf{i}\cdot\mathbf{o}\,\gamma_\rho$. The radius R_D is equal to $|\mathbf{r}_D-\mathbf{r}_0|$, the (dimensionless) detector sensitivity function is given by a_D, and the quantities W_D and $\mathbf{r}_D$ are defined in analogy to the emitter case. The detector integral I_D is also defined analogously to the emitter integral I_E, that is:

$$I_D(\mathbf{r}_0)=\int\int_{A_D}\frac{a_D(\mathbf{r}_D)e^{ik_0|\mathbf{r}_0-\mathbf{r}_D|}}{|\mathbf{r}_0-\mathbf{r}_D|}d^2r_D. \quad (8)$$

Next, the emitter and detector beams are each written in a quasi-plane-wave form,[23] $I_E=p_E(\mathbf{I},\mathbf{r}_0)e^{ik_0(\mathbf{i}\cdot\mathbf{r}_0)}$ and $I_D=p_D(\mathbf{O},\mathbf{r}_0)e^{-ik_0(\mathbf{o}\cdot\mathbf{r}_0)}$, so that Eq. (6) can be expressed

$$N=\frac{k_0^2}{4\pi}\int_{V_0}\Lambda(\mathbf{I},\mathbf{O},\mathbf{r}_0)\;\gamma(\mathbf{r}_0)\;e^{ik_0(\mathbf{i}-\mathbf{o})\cdot\mathbf{r}_0}\,d^3r_0, \quad (9)$$

where the integral is performed over a three-dimensional volume V_0 that contains the entire inhomogeneity γ. Here the measurement system beam function given by

$$\Lambda(\mathbf{I},\mathbf{O},\mathbf{r}_0)=\frac{\rho}{2\pi}\tau(\mathbf{r}_0)p_E(\mathbf{I},\mathbf{r}_0)p_D(\mathbf{O},\mathbf{r}_0) \quad (10)$$

has been introduced. Thus, the measured signal N is a spatial Fourier transform of the medium inhomogeneity function γ weighted by the beam function Λ.

From the mean square magnitude of Eq. (9), the average measured scattered power is expressed

$$\langle|N|^2\rangle=\frac{k_0^4}{16\pi^2}\int_{V_0}\int_{V_1}\Lambda(\mathbf{I},\mathbf{O},\mathbf{r}_0)\Lambda^*(\mathbf{I},\mathbf{O},\mathbf{r}_1)\times\langle\gamma(\mathbf{r}_0)\gamma^*(\mathbf{r}_1)\rangle\;e^{i\mathbf{K}\cdot(\mathbf{r}_0-\mathbf{r}_1)}\,d^3r_1\,d^3r_0, \quad (11)$$

where $\mathbf{K}=k_0(\mathbf{i}-\mathbf{o})$ is the scattering vector.[20,22] The magnitude of the scattering vector corresponding to the principal spatial-frequency content of a given measurement is

$$K=2k_0\,\sin(\theta/2), \quad (12)$$

where θ is the scattering angle.

For random media that are statistically homogeneous, $\langle\gamma(\mathbf{r}_0)\gamma^*(\mathbf{r}_1)\rangle$ is dependent only on the difference between $\mathbf{r}_0$ and $\mathbf{r}_1$, so that the autocorrelation function of the inhomogeneity γ can be written

$$B_\gamma(\mathbf{r}_0-\mathbf{r}_1)=\langle\gamma(\mathbf{r}_0)\gamma^*(\mathbf{r}_1)\rangle.$$

If the autocorrelation function B_γ decays to zero much more rapidly than the beam function $\Lambda(\mathbf{I},\mathbf{O},\mathbf{r}_0)\Lambda^*(\mathbf{I},\mathbf{O},\mathbf{r}_1)$, i.e., if the transducer beam patterns are constant over many correlation volumes of the scattering medium, the average scattered power is given by the expression

$$\langle|N|^2\rangle=\frac{k_0^4}{16\pi^2}\int_{V'}e^{i\mathbf{K}\cdot\mathbf{r}'}\,B_\gamma(\mathbf{r}')d^3r'\times\int_{V_0}|\Lambda(\mathbf{I},\mathbf{O},\mathbf{r}_0)|^2\,d^3r_0, \quad (13)$$

where $\mathbf{r}'=\mathbf{r}_0-\mathbf{r}_1$. The first integral can be interpreted as the power spectrum of the medium variations, $S_\gamma(\mathbf{K})$, as defined in Ref. 25.

Equation (13) can thus be rewritten

$$\frac{k_0^4\pi}{2}S_\gamma(\mathbf{K})=\langle|N|^2\rangle\Big/\int_{V_0}|\Lambda(\mathbf{I},\mathbf{O},\mathbf{r}_0)|^2\,d^3r_0. \quad (14)$$

From Eq. (1), under the Born approximation, the left hand side of Eq. (14) is equal to the differential scattering cross section per unit volume $\overline{\sigma_D}$. Therefore, under the conditions specified in the derivation above, this cross section can be obtained as the power spectrum of the measured signal evaluated at the center frequency, divided by a normalization

factor that describes measurement system effects. This normalization factor can be written

$$J_\Lambda(\mathbf{I},\mathbf{O}) = \int_{V_0} |\Lambda(\mathbf{I},\mathbf{O},\mathbf{r}_0)|^2 \, d^3 r_0 . \tag{15}$$

In the remainder of this section, the details of the evaluation of the system function Λ are presented for the specific case applicable to experiments in which the emitter and detector apertures are composed of unfocused linear elements and the scattering medium is a cylindrical inhomogeneity with tissue-mimicking ultrasonic scattering properties. Since each linear element in the system used for measurements reported here is smaller than a half-wavelength at the system center frequency, the elements are modelled as line sources. Thus, for an aperture consisting of M elements, a_E and a_D in the expressions for I_E and I_D are approximately written as

$$a_{(\cdot)} = \sum_{i=1}^{M} \delta(\sqrt{(y-y_i)^2+(z-z_i)^2}) \; q_i \; u(a-|x|), \tag{16}$$

where $(\cdot)$ is either E or D, and x, y and z represents a three dimensional coordinate system with its origin in the center of the ring transducer, with the z-y plane defining the plane of the ring and x the elevation direction. The coordinates for the ith element in the z-y plane are z_i and y_i. The constants q_i represent the system-dependent amplitude including any apodization, u is the Heaviside step function (defined to be zero for negative arguments and unity for positive arguments), and a is half the element height.

Using Eq. (16), the emitter and detector beams are written as a summation of finite line sources:

$$I_{(\cdot)} = \sum_{i=1}^{M} q_i \int_{-a}^{a} \frac{e^{ik_0\sqrt{(x-x_0)^2+(y-y_i)^2+(z-z_i)^2}}}{\sqrt{(x-x_0)^2+(y-y_i)^2+(z-z_i)^2}} \, dx_0 . \tag{17}$$

The integral in Eq. (17) can be analytically evaluated under a form of the Fresnel approximation valid for $(x-x_0)^2 \ll (y-y_i)^2+(z-z_i)^2$. In this limit, Eq. (17) takes the form

$$I_{(\cdot)} = -\frac{1}{\beta}\sum_{i=1}^{M} q_i \left[\frac{e^{ik_0 R_i}}{R_i} \{C[\beta(x-a)] - C[\beta(x+a)]\} \right.$$
$$\left. + i\{S[\beta(x-a)] - S[\beta(x+a)]\} \right], \tag{18}$$

where $R_i = \sqrt{(y-y_i)^2+(z-z_i)^2}$ and $\beta = \sqrt{k_0/(\pi R_i)}$. The functions C and S are the Fresnel cosine and sine integrals, defined as

$$C(\xi) = \int_0^{\xi} \cos\left(\frac{\pi}{2}\mu^2\right) \, d\mu \tag{19}$$

and

$$S(\xi) = \int_0^{\xi} \sin\left(\frac{\pi}{2}\mu^2\right) \, d\mu . \tag{20}$$

While Eq. (18) can also be expressed in terms of complex Fresnel integrals or complex error functions, the form used above is amenable to computation using available subroutines for evaluation of $C(\xi)$ and $S(\xi)$.

Absorption in the scattering object is included by making the substitutions

$$p_E \rightarrow p_E \times 10^{-\alpha l_E/20}, \quad p_D \rightarrow p_D \times 10^{-\alpha l_D/20}, \tag{21}$$

where α is the ultrasonic absorption in dB/cm and l_E and l_D are distances (in cm) from emitter/detector center to $\mathbf{r}_0$ through the scattering object. The distances were calculated using trigonometric identities and the assumption of a cylindrical scattering volume. Analogous results could also be obtained by use of a complex wave number, with the imaginary part for each frequency employed determined from the absorption at that frequency.

The above derivation includes assumed forms of the emitter amplitude function a_E and the detector sensitivity function a_D. In practice, for an ultrasonic array transducer, these functions are specified electronically as a set of amplitudes and delays, so that the true amplitude and sensitivity are scaled by unknown multiplicative constants dependent on the electromechanical transfer functions of the electronics and transducer elements employed. For absolute measurement of differential scattering cross section per unit volume, these unknown constants can be removed by the calibration technique noted below.

This calibration technique is based on calculation and measurement of the acoustic power transmitted across the ring transducer with the emitter and detector apertures facing one another. The theoretical value for the transmitted power integrated over the detector surface, with all quantities defined analogously to those in the above derivation, is

$$N_T = \frac{\rho}{2\pi} \, \tau(0) \int_{A_D} I_E(\mathbf{r}_D) \; a_D(\mathbf{r}_D) \; d^2 r_D . \tag{22}$$

The differential scattering cross section per unit volume is then written

$$\overline{\sigma}_d(\mathbf{K}) = \frac{|f_s(\omega_0,\mathbf{K})|^2}{|f_T(\omega_0)|^2} \frac{|N_T(\omega_0)|^2}{J_\Lambda(\mathbf{I},\mathbf{O})}, \tag{23}$$

where f_s is the measured scattering amplitude and f_T is the measured amplitude for a directly transmitted wave.

To obtain the normalization functions employed here, the computational method outlined above was implemented as follows. The beam functions from Eq. (18) were numerically computed and spatially weighted by the absorption correction of Eq. (21) for a cylindrical volume that spanned 50 mm in diameter and 30 mm in the axial direction. The resulting beam cross section was then numerically integrated to obtain the normalization factor J_Λ. Equation (22) was also numerically evaluated for a medium without any absorption so that the normalization factor $J_\Lambda/|N_T|^2$, given by Eq. (23), could be obtained.

II. METHODS

Various phantoms consisting of glass spheres in solidified agar were made for the experiments. The phantoms had a cylindrical shape with a diameter of 48 mm and a length of

about 100 mm. Each was molded on a holder that fit a stepper motor fixture so that different circular cross sections along the axis could be scanned.

The production of agar phantoms has been described previously,[29] and a similar method was employed here. A solution consisting of 40 grams of agar (Bacto-Agar, Difco Laboratories, Detroit, MI) per liter water was heated to 90 °C. After the solution had clarified, 4 grams of glass spheres (type A2429 glass, Potters Industries, Valley Forge, PA) per liter were added. The spheres were sieved to have diameters between 75 and 90 μm. The solution was allowed to cool down to 60 °C. Prior to pouring the solution into a mold, 13.4 ml 37% formaldehyde solution (for preservation) was added for each liter of agar solution. To avoid settling of the glass beads, the mold was rotated while the agar was solidifying. ''Sparse'' phantoms were also constructed in an analogous manner except for the use of 0.4 grams of glass spheres per liter. All phantoms were imaged with a commercial ultrasound scanner and a 7 MHz probe to check for flaws and for a uniform sphere distribution.

The density of the phantom was determined by direct measurements of the weight and the volume of a cylindrical sample, and was found to be 1.015 ($\pm$0.005) g/cm^3. The average number density of spheres in the phantoms was 5.37/mm^3 for the dense phantom and 0.537/mm^3 for the sparse phantom. These number densities were calculated from the weight of glass spheres added to the total volume, an assumed mean diameter of 83 μm, and the density of the glass, 2.489 g/cm^3.

The attenuation coefficient for the dense phantom was measured by radiation force at frequencies 0.5 MHz, 1.0 MHz, 2.25 MHz, 3.5 MHz, 5.0 MHz, and 7.5 MHz. The exponential attenuation of best fit was found by a least-squares technique to be $0.032f^{1.84}$ dB/(MHz$^{1.84}\cdot$cm) (f in MHz, at 17 °C). To investigate the influence of the glass beads on the attenuation, an analogous measurement was also made for a sample without glass beads. The exponential fit yielded $0.045f^{1.31}$ dB/(MHz$^{1.31}\cdot$cm) in this case. The calculated exponential attenuation curves gave attenuation values at 2.5 MHz of 0.173 dB/cm for the glass sphere medium and 0.149 dB/cm for the background material. Plots of the measured attenuation values and exponential fits are shown in Fig. 3. The sound speed, measured using a pulse-echo configuration, was 1516 ($\pm$5) m/s at 30.0 °C. For comparison, the corresponding values for pure water are 1510 m/s and 0.9956 g/cm^3 at 30.0 °C. Attenuation was not measured for the sparse phantom.

Using these parameters for speed and density, the plane-wave, normal-incidence, pressure reflection coefficient for the dense phantom is estimated as

$$\Re_p=\frac{\rho_p c_p-\rho_0 c_0}{\rho_p c_p+\rho_0 c_0}\approx 0.0116, \tag{24}$$

where ρ_p and c_p are the measured density and sound speed for the dense phantom and ρ_0 and c_0 are the corresponding values for water at 30.0 °C. Since, therefore, only a small fraction of the incident pressure was reflected from the phantoms, the calculated internal pressure fields used in the normalization were not corrected for these reflection effects.

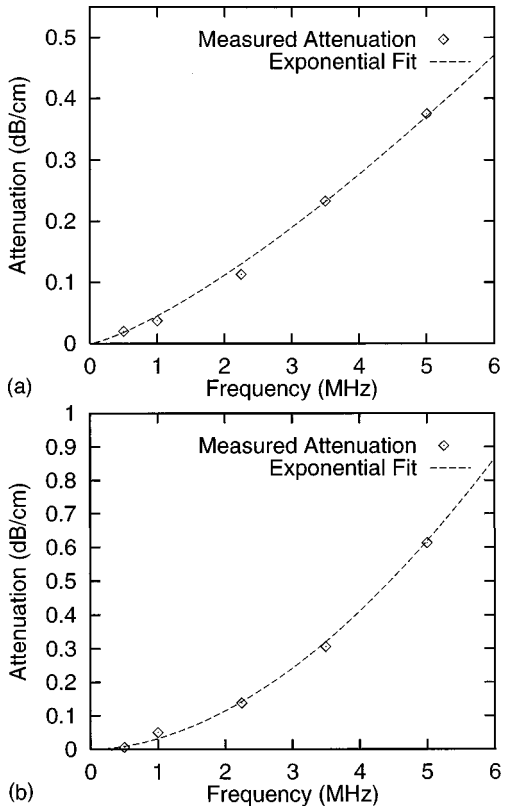

FIG. 3. Measured attenuation and exponential fits. Attenuation values are plotted as points and the corresponding power-law curve fits are plotted as dashed curves. (a) Pure agar. (b) Agar with 5.34 glass spheres per cubic millimeter.

The measured scattered intensity from a distribution of small spheres can be considered to be the sum of the scattered intensity from each sphere if the mean distance between scatterers is sufficiently large that spatial correlation effects are negligible. The theoretical scattered pressure from a single small elastic sphere was calculated using the analytic formula derived by Faran.[30] To obtain a theoretical prediction of the average differential scattering cross section per unit volume for the phantom, the size distribution of the spheres was determined with a Coulter Counter® and the theoretical scattered pressure amplitude was calculated for 28 sphere diameters linearly spaced between 41 μm and 122 μm. The radii measured by this counter are accurate to within error bounds of about 10%. Glass parameters employed in this calculation included a compressional wave speed of 5.572 mm/μs, a shear wave speed of 3.376 mm/μs, and a density of 2.489 g/cm^3. A weighted average amplitude was then found using the measured distribution of sizes. The diameter distribution employed in this calculation is plotted in Fig. 4 as a histogram with 28 bins having centers between 41 μm and 122 μm. The shape of this histogram is consistent with the 75 μm and 90 μm sieve sizes used to sort the spheres, given the limited precision of the counter employed.

The differential scattering cross section per unit volume for the distribution was obtained using the relation

$$\overline{\sigma}_D=\frac{|p_s|^2}{|p_i|^2}R^2 n, \tag{25}$$

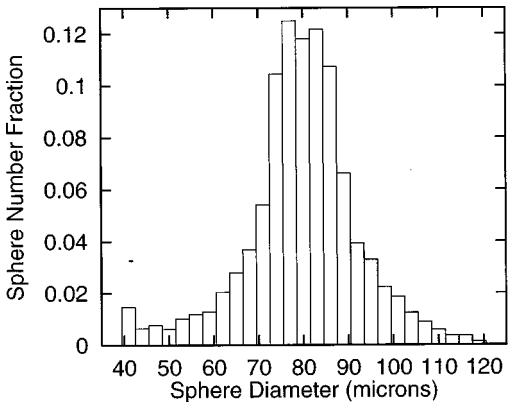

FIG. 4. Histogram of glass sphere diameters measured with Coulter Counter.

where $|p_s|$ is the weighted average scattered pressure amplitude for the sphere distribution, n is the number density of glass spheres, and R is the measurement radius. Plots of the theoretical values for $\overline{\sigma}_D$ are shown in Fig. 5. The corresponding total scattering cross section, defined as the total scattered power for unit incident intensity and unit scatterer volume, is

$$\overline{\sigma} = 2\pi \int_0^{\pi} \overline{\sigma}_D(\theta) \sin(\theta)\, d\theta. \tag{26}$$

The effect of scattering on transmission loss was calculated using the assumption that no power is scattered in the forward direction by the glass sphere distribution. Inspection of Fig. 5 confirms that this assumption is reasonable. Since the fractional power loss due to scattering per unit propagation length is simply $1-\overline{\sigma}$, the contribution of scattering to the measured attenuation per unit length is given in dB by the formula

$$\alpha_{\text{scat}} = 10 \log_{10}(1-\overline{\sigma}), \tag{27}$$

where $\overline{\sigma}$ is the total scattering cross section. Addition of theoretical values of α_{scat} to measured attenuation for the agar medium resulted in transmission loss values very close to those measured for the dense phantom, as shown in Fig. 6. Since this result implies that the increased transmission loss in the phantom is primarily due to scattering rather than to

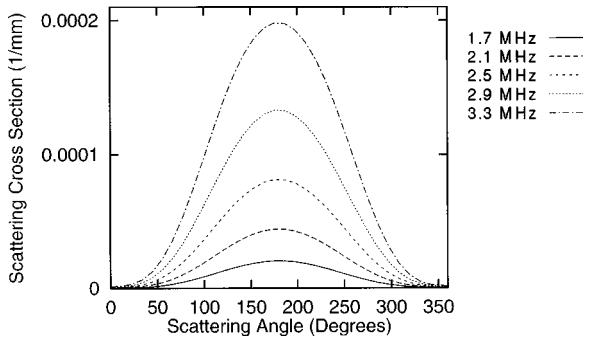

FIG. 5. Theoretical differential scattering cross sections per unit volume for the dense phantom, based on the measured sphere distribution. Cross sections are shown for five incident-wave frequencies between 1.7 MHz and 3.3 MHz.

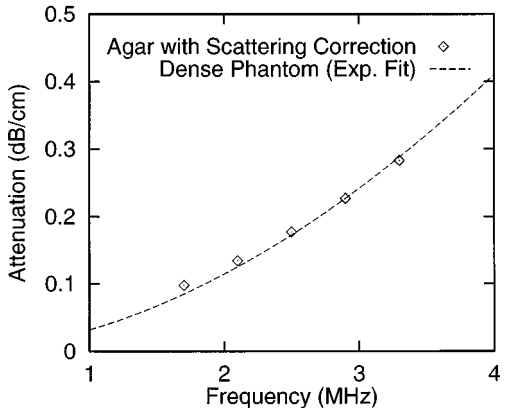

FIG. 6. Effect of scattering on transmission loss. The curve shows the power law of best fit for the dense phantom composed of agar and glass spheres. The data points show calculated values obtained by adding theoretical scattering-induced attenuation to the agar-medium attenuation.

increased absorption, attenuation values measured for the agar background medium were subsequently used for absorption correction in the data analysis.

A transducer array consisting of 2048 elements arranged in a ring with a mean diameter of 150 mm[31] was used for the scattering experiments. Each element in the ring array has an active surface that is 0.23 mm in azimuth and 25 mm in the elevation direction. Transmit signals were synthesized at a rate of 40 MHz with 8-bit resolution and transmitted on 128 contiguous elements, while received signals were sampled at 20 MHz with 12-bit resolution on 16 contiguous elements. The 128-element receiver apertures were synthesized using signals from eight sub-apertures.

Channel-to-channel variations in time delay were compensated using data from a calibration test that employed single-element, broadband, pulse-echo signals recorded from a wire reflector. Variations in channel-to-channel time delay were measured using cross correlation of adjacent signals and were compensated with a channel-to-channel correction of the effective ring radius. All signals measured in the scattering experiments were time shifted according to the delay variations measured in this calibration test.

In the scattering experiments, a plane wavefront was synthesized at the chord of an 128-element wide aperture for both transmit and receive. Thus the wavefront was approximately 29 mm wide. Gaussian apodizations were used so that the transmit and receive beams were smoothly tapered in space. Since the wave space resolution limit, which corresponds to the minimum spatial-frequency scale characterized by a given measurement, is inversely proportional to the second central moment of the beam intersection function,[25] the wide beams and smooth apodizations employed ensured that high wave space resolution was achieved.[25] The standard deviation of the Gaussian apodization functions used was 21.333 elements, or one-sixth the aperture length in azimuth, so that the amplitude at the edge elements was 1.19% of the peak amplitude.

Directly transmitted waves were measured for a water path. At each frequency, the directly transmitted wave (scattering angle 0°) was measured for 64 equally spaced positions around the ring. For each of these transmit positions,

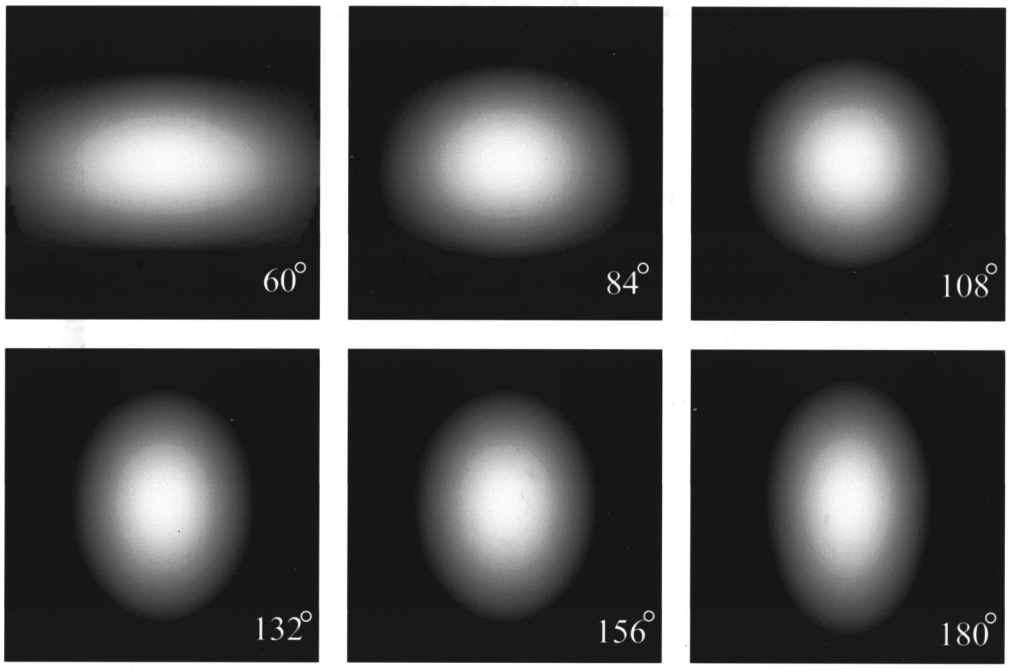

FIG. 7. Beam cross sections. Cross sections of the beam intersection function amplitude in the x-y plane are shown on a logarithmic scale with a 60 dB dynamic range. Beams were calculated for Gaussian apertures, 2.5 MHz center frequency, Gaussian time gates of duration 30 ms and standard deviation 5 ms, and absorption of the agar background medium. Six scattering angles between $\theta = 60°$ (120° between transmitter and receiver) and $\theta = 180°$ (backscatter) are shown. Each plot spans a distance of 50 mm, or one phantom diameter, in height and in width.

scattering data were collected at 49 different receive positions, starting at backscatter and using an angular increment of 2.11° or eight elements. In addition, five phantom elevations separated by about 1 cm were scanned for each temporal elevation, so that $64 \times 5 = 320$ independent measurements were obtained for each scattering angle at each frequency.

Signals from direct-transmission measurements and scattering measurements were gated using Gaussian temporal windows of length 30 μs and standard deviation 5 μs. This signal length corresponds to 75 cycles of a sinusoidal wave at the ring transducer center frequency of 2.5 MHz. The convolution of emitter and detector gates resulted in a spatial window of about 40 mm for scattering angles close to the backscatter direction.

To calculate the differential scattering cross section $\overline{\sigma}_D$, power values for the scattered and transmitted signals were calculated by integrating the signal spectra over a small band around each center frequency. All power values corresponding to equal scattering angles were averaged, so that a single average result was obtained for the transmitted power at each frequency and for scattering measurements at each of 49 scattering angles for each frequency. The scattered signal power was then normalized using Eq. (23) to obtain the differential scattering cross section for each frequency and scattering angle.

For comparison between theoretical and experimental differential scattering cross sections, the experimental cross sections were further normalized by a constant factor determined to match (in the least-square sense) the experimental and theoretical cross sections for the sparse phantom at the center frequency of 2.5 MHz, for scattering angles within $\pm 17°$ of the backscatter direction. The factor, which had a magnitude of 0.5230, was multiplied by the normalized experimental cross sections for both the dense and sparse phantoms. This approach, which is equivalent to the ''reference phantom method'' described in Ref. 32, removed any discrepancies due to inaccuracies in the measured sphere size distribution and in the measured absorption of the agar background medium.

III. RESULTS

Calculated beam pattern cross sections for the center frequency of 2.5 MHz are plotted in Fig. 7 for six scattering angles between 60° (an angle of 120° between emitter and detector) and 180° (backscatter). The beam patterns are seen to have significant support only within the scattering object so that edge effects are minimized. The large apertures, defocused beams, long time gates, and smooth apodization result in slowly varying beams of large spatial extent, so that high wave space resolution is achieved.

A comparison between theoretical and measured beam profiles is shown in Fig. 8 for a center frequency of 2.44 MHz. This figure shows the rms amplitude of the Gaussian transmit beam after direct transmission ($\mathbf{i} = \mathbf{o}$) through a water path. The theoretical transmit beam profile shown was computed using Eqs. (17) and (18) with the weights q_i specified by the plane-wave phase and Gaussian apodization described above; this profile is equivalent to the magnitude of the function $I_E(\mathbf{r}_D)$ that is integrated in Eq. (22) to obtain the transmitted power N_T.

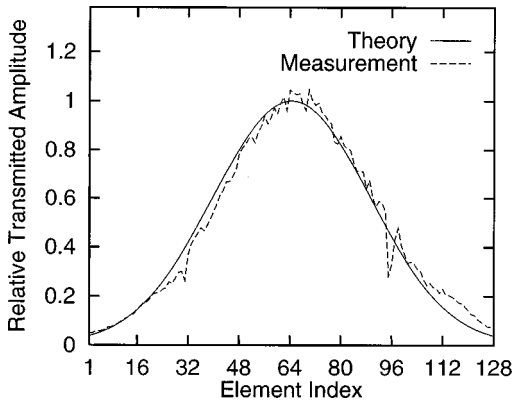

FIG. 8. Computed and measured beam profiles $|I_E(\mathbf{r}_D)|$ for a beam center frequency of 2.44 MHz. These profiles were computed and measured for direct transmission of Gaussian-apodized transmit beams through a water path.

The wave space resolution in each of the directions K_x, K_y, K_z was quantified using the method of Ref. 25 based on the calculated second central moments of the beam intersection function. The angular-dependent 3 dB wave space resolution limits for the center frequency of 2.5 MHz are plotted in Fig. 9. Limits for the other frequencies employed are very close to those for the center frequency, since the beam characteristics depend only weakly on frequency. These results indicate that spatial-frequency features having dimensions on the order of 0.4–1.0 mm^{-1} can be resolved in the present experiments. The spatial-frequency content of each measurement was determined from Eq. (12).

The central spatial frequency interrogated ranged from 1.1 to 4.4 mm^{-1} for the frequencies and scattering angles investigated. The result for the 2.5 MHz measurements is plotted in Fig. 9 together with the corresponding wave space resolution limits. Comparison of these curves indicates that the wave space resolution limit is substantially smaller than the overall spatial-frequency range measured, so that results are not substantially blurred by measurement system effects.

Normalization factors $J_\Lambda/|N_T|^2$ for the agar background medium, determined using Eqs. (15) and (22), are plotted in Fig. 10 for the five frequencies employed. Since the beam

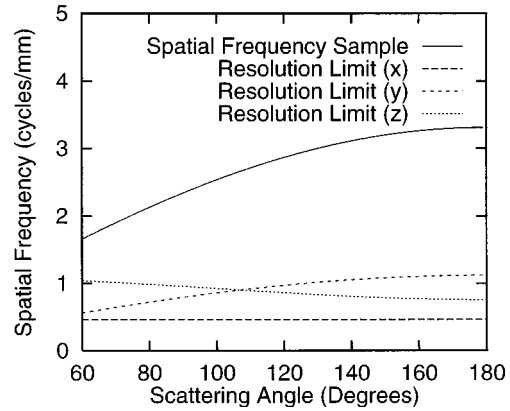

FIG. 9. Spatial-frequency content and wave space resolution limits for scattering measurements using the agar medium. Computed magnitude of the spatial-frequency vector and 3 dB resolution limits in the directions K_x, K_y, and K_z are plotted versus scattering angle for a center frequency of 2.5 MHz.

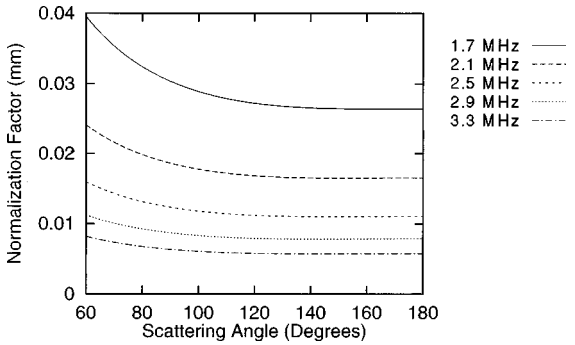

FIG. 10. Computed normalization factors $J_\Lambda/|N_T|^2$ for the agar medium and center frequencies between 1.7 MHz and 3.3 MHz. Beam and time gate parameters are as in Fig. 9.

intersection sizes were comparable for each of the frequencies used, the decrease in the normalization factor with frequency chiefly reflects the increase in ultrasonic absorption with frequency.

Experimentally determined average differential scattering cross sections $\overline{\sigma_D}$ for the dense phantom are plotted in Fig. 11 together with the corresponding theoretical values for the measured distribution of spheres. The measured and theoretical cross sections for the sparse phantom are plotted in Fig. 12. Each plot is shown over the range of scattering angles for which the scattered field was not noticeably influenced by the directly transmitted beam. The angular range is smaller for the sparse phantom because of the smaller scattered power in this case. The experimental values for the dense phantom agree well with theory. Those for the sparse phantom agree fairly well, although some disagreement is evident at the lowest and highest frequencies used as well as at scattering angles furthest from the backscatter direction (180°).

IV. DISCUSSION

The ring transducer configuration employed here is well-suited to *in vitro* characterization of biological tissues, and may be applicable to *in vivo* tissue characterization for organs such as the breast that are accessible for angular scattering measurements. Other organs, such as the liver and kidney, are accessible for a limited range of angles for *in vivo* measurements. Such organs could be directly character-

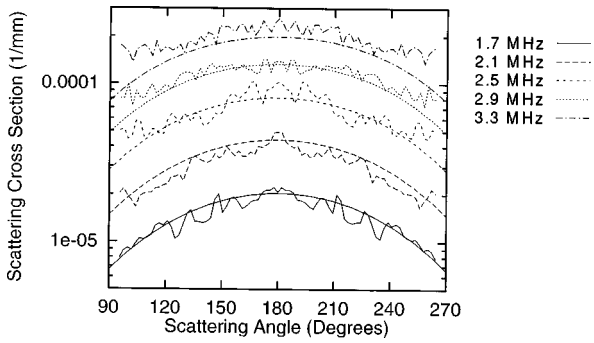

FIG. 11. Measured average differential scattering cross sections for dense glass sphere phantom with theoretical values for random glass sphere distribution.

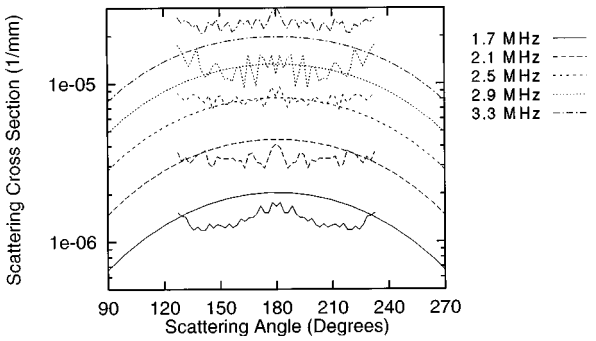

FIG. 12. Measured average differential scattering cross sections for sparse glass sphere phantom with theoretical values for random glass sphere distribution.

ized *in vitro* by the present methods, or could be characterized *in vivo* by a modified measurement configuration employing only backscatter measurements. The methods presented here are fully applicable to backscatter measurements, with the exception that a directly transmitted beam can no longer be employed as a reference. Instead, plane reflectors or reference phantoms of known properties can be employed.[32–34]

The scattering and absorption properties of the phantoms employed here may be compared to measured characteristics of liver tissue.[35] The total scattering cross section for the dense phantom is comparable to the total scattering cross section measured in Ref. 35 for calf liver tissue; however, the absorption of the agar background medium is considerably less than that for calf liver. Thus, for liver tissue, the relative contribution of scattering to attenuation is apparently smaller than that for the dense phantom employed in the present study.

The sparse phantom, which contained one tenth the glass-sphere concentration of the dense phantom, produced much smaller total scattering cross sections than calf liver tissue. Near the backscatter direction, however, the differential scattering cross section for the sparse phantom is comparable to that for calf liver as measured in Ref. 35. For this phantom, greater disagreement between theoretical and experimental cross sections occurs for scattering angles far from backscatter, where the scattered fields are very small. Although system noise may be a factor in these errors, the tendency of disagreement shown in Fig. 12 is for the scattering cross section to be overestimated, indicating that the true scattering signals are obscured by sidelobes of the main beam. These observations imply that the tissue characterization methods presented here may encounter difficulty for characterization of very weakly scattering (hypoechoic) tissue, but that these difficulties may be less important for scattering angles near the backscatter direction.

Broad, unfocused beams and long time gates were used here to achieve maximal wave space resolution. In tissue characterization studies, limiting the spatial extent of insonification may be desirable so that tissue properties can be measured with greater spatial resolution. This trade-off between wave space resolution and spatial resolution is discussed in Ref. 25.

The normalization method employed in this study accounts for the frequency-dependent absorption of the medium. Although the experiments reported here were performed using a weakly absorbing background medium, the employed method of compensation for absorption is also valid for more strongly absorbing media such as tissue.[20] Application of the employed methods to tissue characterization requires estimates of tissue absorption for quantitative accuracy to be achieved. However, since measured data for attenuation in human tissue[36–38] as well as direct methods of attenuation measurement[39,40] are available, this requirement should not greatly limit applicability of the method.

Some error in measurements of scattering cross section can result from inaccurate specification of emitter and detector beams. For instance, the true directivity of the elements employed is not precisely described by the present model of finite line sources in an infinite baffle. However, the agreement of the results obtained with theory suggests that the technique presented here is insensitive to the deviation of element characteristics from this ideal. Other possible sources of error in the measurements include uncertainty in the measured absorption of the agar background medium, neglect of element-response waveform variations in the transducer calibration, and neglect of reflection effects at the agar-water boundary. The most important of these factors is the estimated background absorption, since errors in the absorption contribute exponentially to errors in the measured cross sections.

Although theoretically exact expressions for scattering from glass spheres were employed, the scattering cross sections computed for the measured sphere distributions are still subject to uncertainty. Errors may arise from uncertainties in the electronically counted sphere distribution, which may be suspected because the measured sphere distribution does not precisely match that expected for the sieves employed. Also, the density, longitudinal sound speed, and shear wave speed of the glass spheres were estimated from nominal properties for glass that may not precisely match the spheres employed. Any error in the estimated density of the glass spheres would cause a corresponding error in the estimated number of spheres per unit volume within the phantoms.

The Born approximation was used in the present paper to relate the spatial-frequency properties of the scattering medium to the measured differential scattering cross section. This approximation is based on the assumption that the incident beam is unperturbed by the scattering medium, so that strong scattering, refraction, and diffraction effects are all neglected. Since human soft tissues have been shown to possess ultrasonic scattering properties not fully described by weak scattering approximations,[41] worthy of special note is that measurement of scattering properties employing the techniques developed here is not fundamentally dependent on the Born approximation. Although the present normalization method was derived using the Born approximation, Eq. (23), which expresses a ratio of the total scattered energy to the incident energy, is still valid in the presence of multiple scattering, diffraction, or refraction. However, in situations where the Born approximation does not apply, the relationship between the average differential scattering cross section per unit volume and the spatial-frequency spectra of medium

properties is no longer linear. Furthermore, perturbation of transmit and receive beams by tissue will cause inaccuracy in the estimated beam cross sections required for the normalization method. For scattering by human tissues, therefore, Eq. (14) and similar equations that linearly relate scattered energy to tissue spatial-frequency properties should be regarded as approximations. The utility of these approximations for tissue characterization in strongly inhomogeneous media, such as the human breast, requires further study.

V. CONCLUSION

A method has been presented for the accurate measurement of the angle- and frequency-dependent differential scattering cross sections of random media. General normalization expressions presented were evaluated for the particular case of ultrasonic beams associated with unfocused linear array or phased array transducers, narrow-band emitter signals, and long detector gates. Medium absorption was incorporated explicitly in the normalization.

The method has been applied to an experimental configuration that uses a fixed ring transducer. Beams and time gates were designed for the ring transducer to maximize the achieved wave space resolution of the scattering measurements and to ensure that scattered fields were sampled with high wave space resolution. Normalization expressions were evaluated for the ring transducer configuration using analytic expressions for field patterns of individual elements and numerical inclusion of background medium absorption.

Attenuation measurements for a pure agar medium and for an agar-glass sphere phantom indicate that increased transmission loss in the agar-glass phantom is due to scattering effects rather than to increased absorption. Experimental scattering results for two agar-glass sphere phantoms show good relative agreement with theoretical calculations for measured glass-sphere distributions, although precise comparison between theory and experiment was limited by uncertainties in the background medium absorption, sphere distribution, and the mechanical properties of the glass spheres.

The results show the feasibility for accurate *in vitro* measurements of scattering cross sections using a fixed ring transducer configuration, and suggest that tissue characterization using this method is also feasible.

ACKNOWLEDGMENTS

The authors wish to thank Daofa Zhang, who initially implemented a different method for normalization of the ring transducer scattering measurements, Timothy Heywood and DongLai Liu, whose work on calibration and testing of the ring transducer system was important for this study, Ernest Madsen, who provided valuable advice on phantom construction, and Peter Keng, who helped with use of the Coulter Counter. Helpful discussions with Laura Hinkelman are acknowledged with pleasure. Funding for this work was provided by the University of Rochester Diagnostic Ultrasound Research Laboratory Industrial Associates, NIH Grants Nos. DK 45533 and HL 150855, US Army Grant No. DAMD 17-94-J-4384, the F. V. Hunt Fellowship of the Acoustical Society of America, and the University of Rochester Exchange Visitor Program.

[1] R. Gramiak, R. C. Waag, E. A. Schenk, P. P. K. Lee, K. Thomson, and P. Macintosh, ''Ultrasonic detection of myocardial infarction by amplitude analysis,'' Radiology **130**, 713–720 (1979).
[2] S. A. Wickline, L. J. Thomas III, J. G. Miller, B. E. Sobel, and J. E. Perez, ''A relationship between ultrasonic integrated backscatter and myocardial contractile function,'' J. Clin. Invest. **76**, 2151–2160 (1985).
[3] K. A. Wear, M. R. Milunski, S. A. Wickline, J. E. Perez, B. E. Sobel, and J. G. Miller, ''Differentiation between acutely ischemic myocardium and zones of completed infarction in dogs on the basis of frequency-dependent backscatter,'' J. Acoust. Soc. Am. **85**, 2634–2641 (1989).
[4] J. C. Bamber and C. R. Hill, ''Acoustic properties of normal and cancerous human liver—I. Dependence of pathological conditions,'' Ultrasound Med. Biol. **7**, 121–133 (1981).
[5] R. Momenan, R. F. Wagner, B. S. Garra, M. H. Loew, and M. F. Insana, ''Image staining and differential diagnosis of ultrasound scans based on the Mahalanobis distance,'' IEEE Trans. Med. Imaging **13**, 37–47 (1994).
[6] R. C. Waag and R. M. Lerner, ''Tissue macrostructure determination with swept-frequency ultrasound,'' *IEEE Ultrasonics Symposium Proceedings*, IEEE Cat. No. 73CHO 807-8SU, pp. 63–66 (1973).
[7] R. C. Chivers, R. R. Hill, and D. Nicholas, ''Frequency dependence of ultrasonic backscattering cross-section: An indicator of tissue structure characteristics,'' *Proceedings of the Second World Congress on Ultrasonics in Medicine* (Amsterdam, The Netherlands: Excerpta Medica, 1973), pp. 300–303.
[8] R. A. Sigelmann and J. M. Reid, ''Analysis and measurement of ultrasound backscattering from an ensemble of scatterers excited by sine-wave bursts,'' J. Acoust. Soc. Am. **53**, 1351–1355 (1973).
[9] R. C. Chivers and C. R. Hill, ''A spectral approach to ultrasonic scattering from human tissue: methods, objectives, and backscattering measurements,'' Phys. Med. Biol. **20**, 799–815 (1975).
[10] D. Nicholas, ''Orientation and frequency dependence of backscattered energy and its clinical application,'' in *Recent Advances in Ultrasound in Biomedicine*, edited by D. N. White (Research Studies, Forest Grove, OR, 1977), pp. 29–54.
[11] R. C. Waag, R. M. Lerner, P. P. K. Lee, and R. Gramiak, ''Ultrasonic Diffraction Characterization of Tissue,'' in *Recent Advances in Ultrasound in Biomedicine*, Vol. 1, edited by D. N. White (Research Studies, Forest Grove, OR, 1977), pp. 87–116.
[12] M. O'Donnell and J. G. Miller, ''Quantitative broadband ultrasonic backscatter: An approach to nondestructive evaluation in acoustically inhomogeneous materials,'' J. Appl. Phys. **52**, 1056–1065 (1981).
[13] D. Nicholas, C. R. Hill, and D. K. Nassiri, ''Evaluation of backscattering coefficients for excised human tissues: Principles and techniques,'' Ultrasound Med. Biol. **8**, 7–15 (1982).
[14] F. L. Lizzi, M. Greenebaum, E. J. Feleppa, M. Elbaum, and D. J. Coleman, ''Theoretical framework for spectrum analysis in ultrasonic tissue characterization,'' J. Acoust. Soc. Am. **73**, 1366–1373 (1983).
[15] M. A. Fink and J. F. Cardoso, ''Diffraction effects in pulse-echo measurements,'' IEEE Trans. Sonics Ultrason. **SU-31**, 313–329 (1984).
[16] E. L. Madsen, M. F. Insana, and J. A. Zagzebski, ''Method of data reduction for accurate determination of acoustic backscatter coefficients,'' J. Acoust. Soc. Am. **76**, 913–923 (1984).
[17] M. F. Insana, R. F. Wagner, D. G. Brown, and T. J. Hall, ''Describing small-scale structure in random media using pulse-echo ultrasound,'' J. Acoust. Soc. Am. **87**, 179–192 (1990).
[18] M. F. Insana, T. J. Hall, and L. T. Cook, ''Backscatter coefficient estimation using array transducers,'' IEEE Trans. Ultrason. Ferroelectr. Freq. Control **41**, 714–723 (1994).
[19] J. Meunier and M. Bertrand, ''Echographic image mean gray level changes with tissue dynamics: A system-based model study,'' IEEE Trans. Biomed. Eng. **42**, 403–410 (1995).
[20] J. A. Campbell and R. C. Waag, ''Normalization of ultrasonic scattering measurements to obtain average differential scattering cross sections for tissues,'' J. Acoust. Soc. Am. **74**, 393–399 (1983).
[21] D. K. Nassiri and C. R. Hill, ''The differential and total bulk acoustic scattering cross sections of some human and animal tissues,'' J. Acoust. Soc. Am. **79**, 2034–2047 (1986).
[22] R. C. Waag and J. P. Astheimer, ''Characterization of measurement sys-

tem effects in ultrasonic scattering experiments,'' J. Acoust. Soc. Am. **88**, 2418–2436 (1990).
[23] R. C. Waag, J. P. Astheimer, and J. F. Smith III, ''Analysis and computations of measurement system effects in ultrasonic scattering experiments,'' J. Acoust. Soc. Am. **91**, 1284–1297 (1992).
[24] K. Chandra and C. Thompson, ''Ultrasonic characterization of fractal media,'' Proc. IEEE **81**, 1523–1533 (1993).
[25] T. D. Mast and R. C. Waag, ''Wave space resolution in ultrasonic scattering measurements,'' J. Acoust. Soc. Am. **98**, 3050–3058 (1995).
[26] P. M. Morse and K. U. Ingard, *Theoretical Acoustics* (McGraw-Hill, New York, 1968), Chap. 8.
[27] P. M. Morse and H. Feshbach, *Methods of Theoretical Physics*, *Part I* (McGraw-Hill, New York, 1953), pp. 834–838.
[28] A. D. Pierce, *Acoustics* (McGraw-Hill, New York, 1981), p. 214.
[29] M. M. Burlew, E. L. Madsen, J. A. Zagzebski, R. A. Banjavic, and S. W. Sum, ''A new ultrasound tissue-equivalent material,'' Radiology **134**, 517–520 (1980).
[30] J. J. Faran, ''Sound scattering by solid cylinders and spheres,'' J. Acoust. Soc. Am. **23**, 405–418 (1951).
[31] R. C. Waag, D.-L. Liu, T. D. Mast, A. I. Nachman, P. Jaeger, and T. Kojima, ''An ultrasonic ring transducer system for studies of scattering and imaging,'' J. Acoust. Soc. Am. **100**, 2795 (1996).
[32] J. A. Zagzebski, L. X. Xao, E. J. Boote, and Z. F. Lu, ''Quantitative backscatter imaging,'' in *Ultrasonic Scattering in Biological Tissues*, edited by K. K. Shung and G. A. Thieme (CRC, Boca Raton, 1993), pp. 451–486.
[33] K. J. Peters and R. C. Waag, ''Compensation for receiver bandpass effects on backscatter power spectra using a random medium model,'' J. Acoust. Soc. Am. **84**, 392–399 (1988).
[34] J. M. Reid, ''Standard substitution methods for measuring ultrasonic scattering in tissues,'' in *Ultrasonic Scattering in Biological Tissues*, edited by K. K. Shung and G. A. Thieme (CRC, Boca Raton, 1993), pp. 171–204.
[35] J. A. Campbell and R. C. Waag, ''Measurements of calf liver ultrasonic differential and total scattering cross sections,'' J. Acoust. Soc. Am. **75**, 603–611 (1984).
[36] S. A. Goss, R. L. Johnston, and F. Dunn, ''Comprehensive compilation of empirical ultrasonic properties of mammalian tissues,'' J. Acoust. Soc. Am. **64**, 423–457 (1978).
[37] S. A. Goss, R. L. Johnston, and F. Dunn, ''Compilation of empirical ultrasonic properties of mammalian tissues II,'' J. Acoust. Soc. Am. **68**, 93–108 (1980).
[38] F. A. Duck, *Physical Properties of Tissue: a Comprehensive Reference Book* (Academic, New York, 1990).
[39] K. J. Parker, R. M. Lerner, and R. C. Waag, ''Comparison of techniques for *in vivo* attenuation measurements,'' IEEE Trans. Biomed. Eng. **35**, 1064–1068 (1988).
[40] E. L. Madsen, ''Method of determination of acoustic backscatter and attenuation coefficients independent of depth and instrumentation,'' in *Ultrasonic Scattering in Biological Tissues*, edited by K. K. Shung and G. A. Thieme (CRC, Boca Raton, 1993), pp. 205–250.
[41] T. D. Mast, L. M. Hinkelman, M. J. Orr, V. W. Sparrow, and R. C. Waag, ''Simulation of ultrasonic pulse propagation through the abdominal wall,'' J. Acoust. Soc. Am. **102**, 1177–1190 (1997).